Identification of cholesteryl esters in human carotid atherosclerosis by ex vivo image-guided proton MRS

Frederick L. Ruberg,* Jason Viereck,†,§ Alkystis Phinikaridou,† Ye Qiao,† Joseph Loscalzo,* and James A. Hamilton,[1,†]

Whitaker Cardiovascular Institute, Evans Department of Medicine and Section of Cardiology,* Department of Physiology and Biophysics,† and Department of Neurology,§ Boston University School of Medicine, Boston, MA

Abstract Vulnerable atherosclerotic plaques may be identified by their large lipid component, particularly liquid cholesteryl ester (CE), covered by a fibrous cap. We hypothesized that image-guided ^{1}H proton magnetic resonance spectroscopy (MRS) would identify mobile CE in discrete, preselected regions of atherosclerotic plaque. Human carotid endarterectomy specimens (n = 10) were imaged ex vivo by magnetic resonance imaging (MRI) at high field (11.7 T) utilizing standard T1- and T2-weighted spin echo protocols. MRS spectra were acquired from 1 mm^3 voxels, localized to plaque regions that we judged by MRI to be lipid rich or lipid poor. The spectra revealed methyl and methylene resonances of fatty acyl chains with relative intensities and linewidths characteristic of pure CE, by comparison with lipid standards. Regions judged to be lipid rich by MRI showed much more intense CE resonances than did lipid-poor regions. The integrated intensities of lipid peaks were 5.5 ± 2.0% (lipid-rich regions) versus 0.9 ± 0.6% (lipid-poor regions) of the unsuppressed water peak ($P < 0.0001$). Lipid distribution by histology, MRS, and MRI showed strong correlation. Image-guided proton MRS accurately identified CE in selected regions of atherosclerotic plaque as small as 1 mm^3 in an ex vivo setting. This procedure may permit the noninvasive detection and quantification of CE in atherosclerotic plaque in vivo.— Ruberg, F. L., J. Viereck, A. Phinikaridou, Y. Qiao, J. Loscalzo, and J. A. Hamilton. **Identification of cholesteryl esters in human carotid atherosclerosis by ex vivo image-guided proton MRS. *J. Lipid Res.* 2006.** 47: **310–317.**

Supplementary key words magnetic resonance spectroscopy • stroke • vulnerable plaque • plaque lipids

The transformation of a quiescent atherosclerotic plaque to an active plaque leads to acute ischemic syndromes, such as myocardial infarction and stroke (1). Although the cascade of events that ultimately results in a vulnerable plaque is not completely known, histology studies have demonstrated typical features of the vulnerable plaque to include a large lipid core subscribed by a thin collagen cap (2). Thus, a vulnerable plaque might be identified prior to an atherothrombotic complication if one or more of these distinguishing features could be identified in vivo. Catheter-based techniques such as intravascular ultrasound (IVUS), optical coherence tomography (OCT), near infrared spectroscopy, and Raman spectroscopy are able to identify specific plaque elements, such as the lipid core, but their use in humans is limited by their invasive nature (3, 4). Magnetic resonance imaging (MRI) can identify specific plaque components noninvasively through signal intensity differences elicited by varying contrast-weighted sequences (5, 6). Accentuating inherent differences in the proton relaxation properties of plaque components, including lipid, blood, fibrous tissue, and free water, MRI can afford near-histological resolution ex vivo without sample destruction (7–9). Although some plaque components can be identified, the detection of plaque lipid by MRI can be limited because lipid regions are inhomogeneous. Furthermore, lipid regions may contain crystals of cholesterol, and are sometimes proximal to regions of calcification, both of which create a signal void in proton MRI. To enhance detection of lipids, some investigators have employed gadolinium contrast enhancement to identify lipid with greater sensitivity (10, 11), although this approach relies on relatively nonspecific signal intensity properties and individual lipid species are not identified.

Cholesteryl ester (CE) in the liquid phase comprises a major fraction of the lipid-rich core of the plaque, and its abundance has been associated with plaque rupture and formation of atherothrombosis (12). The unique lipid composition of the plaque, with the high proportion of CE relative to other lipids, is mainly a result of the infiltration and retention of the plasma lipoprotein LDL (13–15). Oxidative modification of the lipoprotein-derived CE (16) may constitute an important chemical contributor to the

Manuscript received 29 September 2005 and in revised form 8 November 2005.

Published, JLR Papers in Press, November 29, 2005.
DOI 10.1194/jlr.M500431-JLR200

Abbreviations: CE, cholesteryl ester; CSI, chemical shift imaging; FOV, field of view; IVUS, intravascular ultrasound; MRS, magnetic resonance spectroscopy; OCT, optical coherence tomography; T1W, T1-weighted; TG, triacylglycerol; TR, repetition time.

[1] To whom correspondence should be addressed.
e-mail: jhamilt@bu.edu

development of rupture. In addition, the proximity of liquid CE to other plaque components, such as the fibrous cap, has been postulated to be important for plaque stability (17). Image-guided proton ^{1}H magnetic resonance spectroscopy (MRS) has the potential to detect liquid CE noninvasively, with a high degree of sensitivity and spatial resolution, and without the need for additional contrast agents. Unlike MRI, which creates an image pixel using the sum of signals from all proton resonances in a given volume, MRS gives a spectrum of resonances, thus affording detection of specific chemical components through their inherent frequency shift relative to water (18). In image-guided MRS, an MR image can be utilized to select specific plaque regions that appear either lipid rich or lipid poor by MR imaging characteristics alone. Proton spectra can then be collected from these regions of interest, or voxels, such that the specific proton resonances of lipid components in a mobile state, including CE, can be identified.

An overall goal in our studies of plaque pathology and atherothrombosis is to develop imaging methods and spectroscopy approaches that will detect specific chemical components in plaques and will have the potential for in vivo applications. We present here the first application of image-guided single-voxel proton MRS in the identification of liquid CE in ex vivo carotid specimens acquired from patients with transient ischemic attack or stroke. Proton MRS in volumes as small as 1 mm^3 confirmed the presence and abundance of CE in regions suggested by MR images to be lipid rich. Although these studies were performed ex vivo, successful translation of this technique in vivo may afford precise identification of plaque lipid species and permit noninvasive detection of lipid features typical of vulnerable plaque.

MATERIALS AND METHODS

Specimens

Patients with ipsilateral ischemic complications (transient ischemic attack or stroke) resulting from carotid atherosclerotic stenosis were identified prior to carotid endarterectomy. Carotid specimens following surgery were obtained with approval from the Institutional Review Board of Boston University Medical Center in a de-identified manner, such that additional demographic and medical history was unavailable. Specimens (n = 10) were transported from the operating room at room temperature and then placed in phosphate-buffered saline containing 1:100 dilution protease inhibitor cocktail (Sigma-Aldrich; St. Louis, MO) and stored at 4°C until imaging and spectroscopic studies. Imaging and spectroscopy were usually performed 24 h–48 h following acquisition of the specimen. It has been shown previously that that the T1 and T2 relaxation times of arterial plaques remained essentially unchanged when preserved at 4°C for up to 7 days and then warmed to 37°C for relaxation time measurements, which indicates that there is no change in the mobile lipids (19). Specimens were placed in a graduated MR-compatible tube for registration with histological sectioning.

Preparation of standards

CE (linoleate), triacylglycerol (TG; olive oil), and phospholipid (egg phosphatidylcholine) were purchased from Sigma-Aldrich. Standards were prepared to verify the fidelity of spectra acquired by the image-guided single-voxel technique, as compared with published standards. Cholesteryl linoleate is the most abundant CE in advanced plaques (12), and olive oil is rich in oleic acid, a common fatty acid in TG. Cholesteryl linoleate was heated to 45°C to ensure complete melting (crystal-to-isotropic transition = 42°C), then permitted to cool inside the probe to physiological temperature (37°C), just above isotropic-to-cholesteric liquid crystalline phase transition, at which temperature images and spectra were obtained. Triglyceride standards were heated to 37°C and analyzed directly. Phospholipid standards were hydrated to 70% by weight at room temperature for 48 h and then subjected to five freeze–thaw cycles in liquid nitrogen, followed by vortexing to ensure sample homogeneity.

MRI

MRI was performed at 11.7 T using a vertical-bore Bruker Biospec 500 MHz spectrometer (Bruker; Billerica, MA) fitted with gradient coils to permit imaging. The imager was controlled by Paravision© software (Bruker) running on a Silicon Graphics O2 computer (Silicon Graphics; Mountain View, CA). Specimens were placed in either 10 mm or 20 mm diameter imaging coils and loaded into the isocenter of the magnet. Specimens were heated by air exchange to 37°C 20 min prior to initiation of the imaging protocol to permit thermal equilibration. High-resolution images were acquired from 1 mm thick axial slices utilizing T1-weighted (T1W) and T2-weighted (T2W) spin echo protocols (Bruker sequence MSME_BIO). T1W parameters were: matrix, 256 × 256; field of view (FOV), 1.5 cm; repetition time (TR), 300–500 ms; echo time (TE), 15 ms. T2W parameters were: matrix, 256 × 256; FOV, 1.5 cm; TR, 2,000 ms; TE, 30 ms. In-plane resolution was 60 μm (FOV/matrix). The time needed to acquire a complete set of either T1W or T2W images was typically between 45 to 60 min. Following image acquisition, a colorized polar map of the ratio of T1/T2 image intensity (based solely upon signal and dependent upon T1/T2 contrast weighting) was generated using the algebraic function of Paravision. This polar map highlighted signal intensity differences between the T1 and T2 images and was utilized to select regions for proton spectroscopy.

MRS

Image-guided proton MRS was performed following MRI and identification of plaque regions that appeared either lipid rich or lipid poor by intensity polar mapping. Spectra were acquired from 1 mm^3 voxels using the PRESS technique (point-resolved spectroscopy) of voxel selection (Bruker sequence VSEL_SE_SPEC). Following identification of the region of interest, a larger 5 mm^3 voxel was placed over the region to permit shimming of B_0 on the water peak and optimization of the 90° and 180° pulses. The water signal was then selectively suppressed by presaturation. This procedure was performed at the onset of experimentation for each specimen, with shimming optimization repeated only when the region of interest moved outside the initial shimming volume. Voxel size was then reduced to 1 mm^3 and localized to the region of interest. Spectroscopy parameters were as follows: spectral width, 10 K; acquisition size, 2048; TR, 500 ms; TE, 15 ms; and Number of Excitations (NEX), 600. Additional spectroscopic measurements were made with identical parameters except for TR of 2,000 ms. Spectral acquisition time was 5 min. A second spectrum from the same voxel position was acquired without water suppression for standardization. This technique of voxel selection and signal acquisition was applied to phantom samples of pure CE and TG to test the sensitivity of the technique and the accuracy of voxel selection. Following acquisition, spectra were manually phase corrected and postprocessed using XWIN-NMR©

(Bruker), and compared with published standards to permit peak assignment (20). The water peak was assigned to 4.7 ppm. Methyl and methylene resonances of fatty acyl chains were identified in their characteristic spectral region (0.8 ppm–1.4 ppm). A lipid:water ratio was calculated to permit semiquantitative comparison between different voxel regions by taking the integrated area subscribed by the peak methyl and methylene resonances and expressing it as a fraction of the integrated water peak without presaturation (assigned to 1.0). Ratios from a priori-identified lipid-rich and lipid-poor plaque regions were compared statistically using an unpaired Student's *t*-test.

Voxel-defined MRS was also performed on standards of purified CE (cholesteryl linoleate; Sigma-Aldrich) and TG (triolein).

Histology and sample registration

Following MRI and MRS, specimens were cryogenically sectioned for polarized light microscopy (21) and stained for plaque components with oil red O. Histology specimens, MR image slices, and spectral voxels were matched both visually and by employing the graduations printed on the imaging tube. Orientation during imaging and histological sectioning was maintained. Measurement from the end of the specimen during histological sectioning permitted accurate co-registration.

RESULTS

MRS of standards

As an initial demonstration of the efficacy of this technique, as well as to optimize pulse sequence parameters, image-guided proton MRS was performed on prepared standards of the lipid species of atherosclerotic plaque, including purified CE, triglyceride, and phospholipid. **Figure 1** illustrates typical proton spectra from phospholipid in panel A, TG in panel B, and CE in panel C, obtained from the voxel illustrated for each standard. In the phospholipid spectrum (A) the only observed resonance is from water (4.7 ppm) added to the dry phospholipid to prepare hydrated mutilayers, which serve as models of cell membranes or aggregated phospholipids. No resonances from the phospholipid were observed, as expected because of their highly restricted and anisotropic motions in the liquid crystalline multilayer. In contrast, spectra from TG (B) and CE (C) showed intense resonances from the methyl (0.8 ppm) and methylene (1.2 ppm) protons of fatty acyl chains. Unique identifiers of specific lipid species (glyceryl CH and CH_2 groups for TG, and the angular methyls and the methine proton from the C3 position for CE) are evident in the lipid standards but are very weak and may not be detected in atherosclerotic plaques. Without these unique identifiers, distinction between CE and TG can be made in model mixtures on the basis of the intensity ratio of the methyl region (0.8 ppm) to the methylene region (1.2 ppm).

MRS detection of CE in MRI-determined lipid-rich regions

MR images obtained for all 10 excised carotid plaque specimens suggested the presence of lipid-rich and lipid-

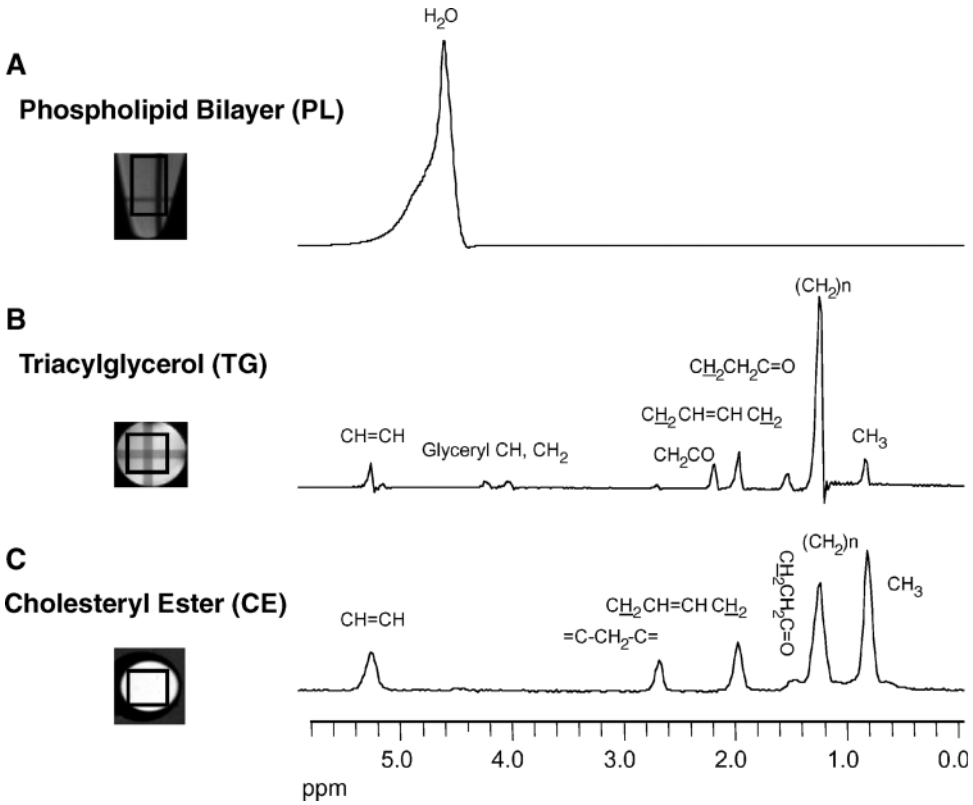

Fig. 1. Proton spectra from lipid standards are illustrated with assignments of the major peaks. A: Hydrated phospholipid (PL) bilayers. B: Pure triacylglycerol (TG). C: Cholesteryl ester (CE). Standards are shown with the MR image inset to the left, in which the voxel selected for spectral analysis is outlined.

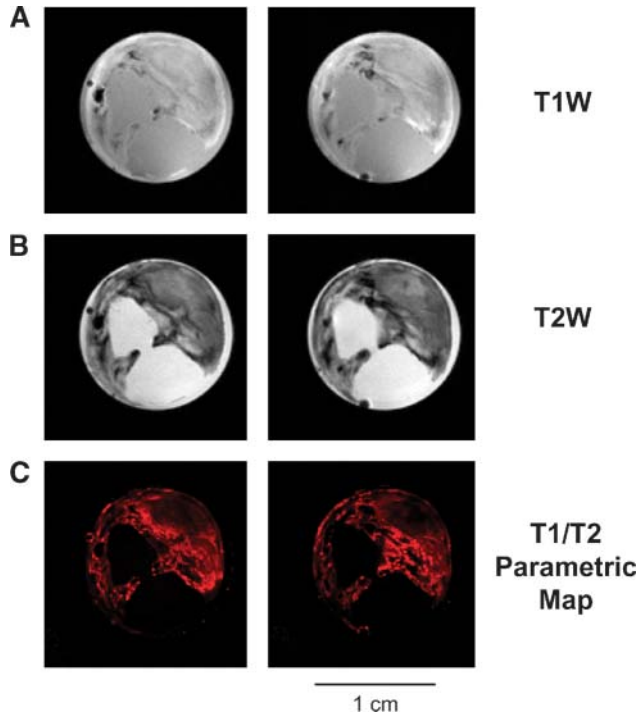

Fig. 2. MR images (two contiguous axial slices) of a carotid plaque ex vivo are shown in each panel, with T1 weighting (A) and T2 weighting (B). C: False-colored parametric map of the ratio of T1-to-T2 image intensity. Lipid-rich regions, characterized by a high T1 relative to T2 intensity, are expected to be bright in this representation. The luminal surface lies inferiorly at the interface of the aqueous buffer.

poor regions. **Figure 2** illustrates a typical result and shows two contiguous axial slices with T1 contrast weighting (A) and the same two slices with T2 contrast weighting (B). Generation of a polar intensity map from the ratio of the T1/T2 images is shown in panel C. This pseudo-colored map highlights differences in imaging intensity. Bright regions (i.e., those with larger differences in T1 vs. T2 signal intensity) were predicted to be lipid rich; lipid-poor regions were judged to be iso-intense to dark (7).

Application of image-guided spectroscopy demonstrated the relative abundance of CE in the a priori-identified lipid-rich or lipid-poor regions selected by the polar map. **Figure 3** illustrates proton spectra from two 1 mm^3 voxels selected from the polar map of Fig. 2. Spectra 3A and 3B were elicited from a lipid-poor region identified by intensity mapping, and spectra 3C and 3D from a lipid-rich region. MRS of other lipid-poor and lipid-rich regions within the same plaque sample gave similar results. For our initial images, a long TR of 2 s was selected to permit maximal T1 signal recovery of protons in water. Spectra obtained without water suppression prepulse (Fig. 3A, C) were obtained to permit standardization and quantitative comparison between different measurements. In this representation, the spectra are not scaled to reflect the absolute intensities of the (suppressed) water signal. Inspection of these spectra yields only a weak lipid signal relative to the water signal. However, with water suppression, intense lipid resonance peaks from the lipid-rich region can be identified readily (Fig. 3D), with the methyl/methylene peak intensity ratio similar to that of pure CE (Fig. 1C). The lipid-poor region gives rise to relatively weak CE peaks (Fig. 3B) that are visible only with expansion (inset). Thus, image-guided proton spectroscopy confirms the presence of CE in lipid-rich regions identified by intensity mapping.

To permit comparison of the lipid content between voxels from the same or different plaque specimens, we modified the above procedures to attenuate the water signal to a degree that would permit better quantification of the lipid signal relative to that of water. We chose to shorten the TR to 500 ms to accentuate the inherent differences between the T1 relaxation of lipid (short) as compared with that of water (long), and thus increase the lipid signal relative to that of water. Using this protocol, quantitative comparison of proton spectra between different plaques was performed by calculating the lipid-to-water peak area ratio for each spectrum. In lipid-rich

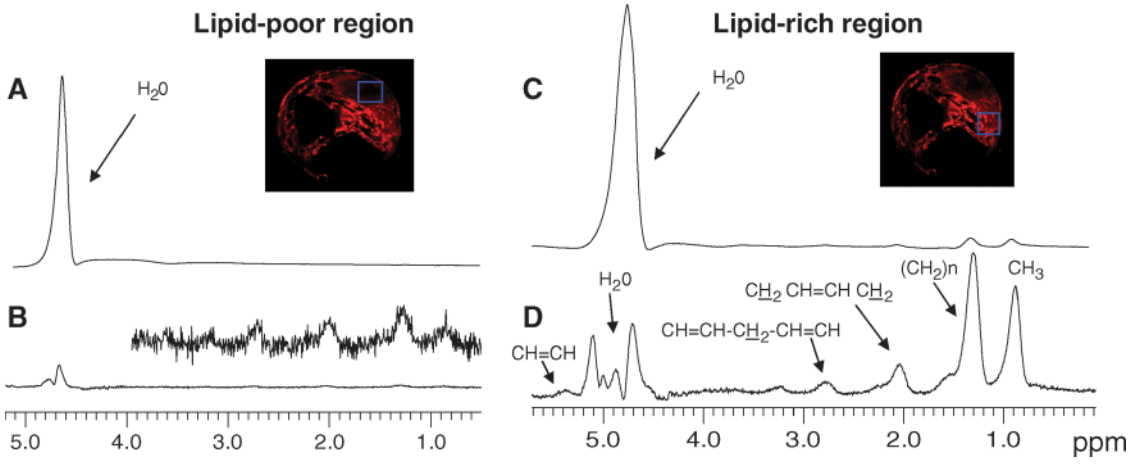

Fig. 3. Spectra elicited from 1 mm^3 voxels are illustrated with insets showing the parametric map and voxel position for reference. A, C: The intense water signal without water suppression. Weak lipid signals are evident (B) only after vertical expansion (inset). In contrast, strong lipid signals (consistent with CE) are seen in D.

regions, the peak intensities corresponding to CE were 5.5 ± 2.0% of the total water signal, whereas in lipid-poor regions, the CE content was only 0.9 ± 0.6% of the total water signal ($P < 0.0001$).

Correlation of MRI, MRS, and histology

To validate further the application of MRS to detect plaque CE, we compared MRI, histology, and spectroscopy in selected samples. **Figure 4** illustrates results for one representative carotid plaque. The T1W (Fig. 4A) and T2W (Fig. 4B) images show a large central region with a signal void that could represent cholesterol crystals or calcification, the latter a common feature of mature carotid plaques (22). The T1/T2 parametric map (Fig. 4C) suggests lipid-rich regions surrounding several dark regions, including the large central region. The histology slice stained with oil red O to detect neutral lipid (Fig. 4D) shows intense red staining for lipid in most of the plaque. The lighter pink regions with diffuse background staining are lipid poor or devoid of lipid. The central region corresponding to the large signal void in the MR images shows a fracture with loss of most of the material in this region, a distortion that is characteristic of calcification rather than of crystalline cholesterol. A polarized light micrograph of a tissue slice (Fig. 4E) contiguous to that obtained for the oil red O staining shows positive (bright) birefringence characteristic of ordered lipid. Under higher magnification and higher temperature (data not shown), most of the birefringence is in droplets, suggesting the presence of CE rather than crystalline cholesterol (12). These bright regions correspond well with the darkest staining areas in the oil red O section. A lipid-rich region identified by MRI (Fig. 4C, right box), and by both types of histology, showed intense lipid resonances with a methyl/methylene peak height ratio and linewidths similar to that of pure CE (Fig. 4F). A spectrum obtained within a relatively dark region of the parametric map (Fig. 4C), box on left side) and shown to be lipid poor by histology revealed relatively weak lipid resonances, as in Fig. 3A (spectrum not shown).

It should be noted that the histological slices and MRI images are not expected to match perfectly for two reasons. First, there is shrinkage of the tissue during preparation for histology. Second, the histology slices are 0.01 mm thick, where the image "slices" are 1.0 mm thick (the width of the square of a voxel for MRS experiments).

DISCUSSION

This study represents the first demonstration of image-guided single-voxel proton MRS applied to atherosclerotic plaque. We first employed imaging signal intensity to create a parametric map of T1 relative to T2 weighting to preselect lipid-rich regions. Then, we were able to confirm the presence of CE using image-guided MRS, and further confirmed the presence of CE through polarized light microscopy following histological sectioning.

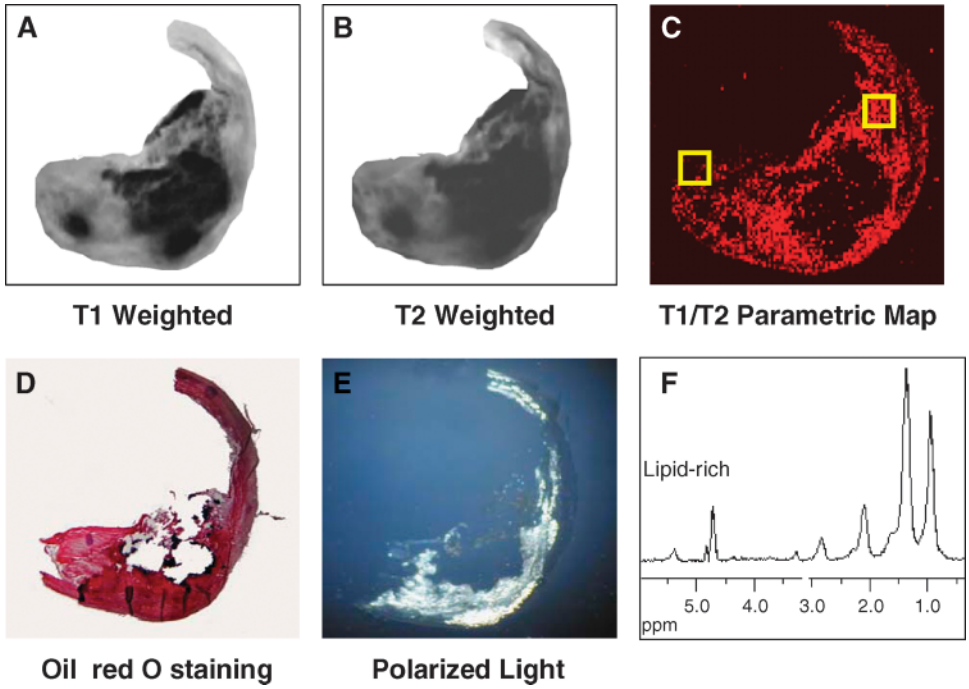

Fig. 4. Axial slices from a different plaque specimen are shown with T1 weighting (A), T2 weighting (B), and parametric intensity map (C). Right yellow box in C is placed over a lipid-rich region; left box over a dark or lipid poor region of the parametric map. Background signal intensity from the buffer solution was manually removed to highlight contrast. D: Co-registered histology slice stained with oil red O. E: Co-registered polarized light micrograph (room temperature). F: Proton spectrum obtained in a 1 mm^3 voxel from a bright region of the parametric map (panel C, right box).

The ability to identify vulnerable plaque noninvasively prior to the occurrence of an atherothrombotic event would represent a significant clinical advance. Because vulnerable plaque has been associated histologically with a large lipid core consisting mostly of CE and unesterified cholesterol, methodologies directed at lipid detection might provide such insight. Indeed, techniques such as IVUS (23) and OCT (24) are particularly useful at identifying plaque lipid. These techniques, however, are limited by their invasive nature and do not identify specific lipid species. MRI can identify specific plaque components, including lipid, noninvasively, but identification is predicated upon relatively nonspecific signal intensity differences seen on proton images acquired through different pulse sequences, with some employing gadolinium contrast (5, 8). Lipid appears bright on T1W images because of the shorter T1 relaxation time of the protons in lipid relative to that of the protons in water; however, other plaque components can also appear bright, including extravasated red blood cells following intraplaque hemorrhage (25). The value of proton MRS is that the signal identifies only mobile lipids. The most abundant mobile lipid in plaques is liquid CE, a lipid that has specifically been linked to plaque rupture, particularly if modified by oxidation (16). MRS affords the potential to directly and unequivocally identify and characterize CE through its specific proton resonances.

Lipid quantification by image-guided proton spectroscopy has been widely applied in vivo to solid organs, including liver and skeletal muscle (26), and more recently to the myocardium (27). In these applications, the lipid consists almost entirely of TG in large droplets, which yields a hyperintense signal on MRI and high signal-to-noise ratios for spectroscopy. Voxel sizes are typically on the scale of $1 \times 1 \times 1$ cm^3 or larger, but MRS has been applied in vivo to voxels as small as $15 \times 15 \times 15$ mm^3 in muscle (28) and $10 \times 20 \times 30$ mm^3 in the heart (27). Although TG and CE (liquid) are essentially indiscernible by MRI, application of MRS can potentially differentiate between these two lipid species in vivo. Measurement of a lipid signal-to-water signal ratio permits comparison between subjects if one assumes the water signal to be relatively similar and measured in the same manner. Numerous studies have demonstrated the efficacy of this technique such that MRS has become an acceptable noninvasive means to determine hepatic TG content (29).

Compared with the liver, the atherosclerotic plaque represents a considerably more challenging target for MRS. It encompasses a very small volume and contains a heterogeneous pool of lipids, in addition to cellular debris, calcium phosphate crystals, and fibrous protein. The quantity of TG within the plaque is very low (ranging from 3% to 6% of total lipids, depending on the classification of the plaque) (30). However, TG adherent to the adventitia (extravascular TG) can contribute to MRS if large voxel sizes are used. The major lipids (CE, cholesterol, and phospholipids) exist in liquid, liquid crystalline, or crystalline states within the plaque. We have performed MRS in extremely small voxel sizes (1 mm^3, a volume almost three orders of magnitude smaller, compared with the liver and muscle studies cited above) to examine lipids in different regions within the plaque and to avert contamination of extravascular TG. Despite the great heterogeneity of the plaque, the proton spectra elicited are quite simple, as illustrated in Fig. 3. This result is predicted from previous applications of "solution state" NMR spectroscopy to biological tissue, which demonstrated that the NMR spectra reflect only the mobile molecules within the plaque, even though the mobile constituents may not be the most abundant constituents (31). The first NMR spectroscopic study of atherosclerotic plaque (ex vivo coronary vessel) revealed a high-resolution ^{13}C NMR spectrum that reflected almost exclusively liquid CE (32). Lipids in liquid crystalline and crystalline phases (phospholipids and cholesterol, respectively) are detected by magic angle spinning ^{13}C NMR (33, 34), a method that does not have potential for in vivo studies because of the requirement for rapid spinning (kHz). Thus, the biophysical properties of the lipids determine their detectability in different NMR experiments and afford the potential in vivo applications of spectroscopy. Only the liquid phase lipids (which consist mainly of CE in the plaque) are detected in the standard spectroscopic experiment that we have applied in this study. Our spectra of the pure lipid standards (Fig. 1) illustrate this point; the ordered phospholipids give rise to no signal, whereas the liquid CE and TG give rise to a high-resolution spectrum. Further studies that we have performed with standard mixtures of CE and TG (not presented here) have yielded a predictable and linear change in lipid methyl peak intensity, permitting relative quantification of these two lipids in a mixture.

It is important to note that previous NMR studies of atherosclerotic plaque lipid in human and animal models have employed the entire plaque specimen, rather than specific, selected regions (35, 36). In addition to image-guided spectroscopy, another approach is chemical shift imaging (CSI), a form of spectroscopic imaging in which specific resonances can be selected and assigned a pixel intensity. CSI of atherosclerotic plaque divides the FOV into a matrix of single voxels and then elicits a spectrum from each (37–40). Although an elegant technique, it lacks the sensitivity of the single-voxel technique, which permits signal averaging from a selected region for a greater signal-to-noise ratio. Another MRI technique used to identify or exclude the presence of lipid is suppression of the lipid resonances by a saturating prepulse prior to the excitation radiofrequency pulse (fat saturation). Although it achieves good results in solid-organ applications in-vivo (heart, liver), its application to atherosclerotic plaque ex-vivo has not been successful. Even if successful in lipid detection, fat suppression techniques, at present, do not permit discrimination of different lipid species.

The present study has a number of limitations when considering the ultimate goal of in vivo translation of this technique. This work was performed under carefully controlled conditions, ex vivo, and at high field (11.7 T), with optimized shimming conditions. Clinical MRI scanners generally operate at a field strength of 1.5 or 3.0 T, affording a lower signal-to-noise ratio, and lack the 3rd- and

4th-order shimming applied in this study. In addition, the barriers to in vivo translation of this technique include subject movement, limitations on scan time, larger voxel selection size, signal contamination by lipid outside the voxel, and field inhomogeneities induced by inflowing blood. We are presently working to overcome these limitations by acquiring in vivo spectra at 3.0 T from voxels localized to the carotid artery in human subjects prior to endarterectomy. Preliminary results demonstrate the feasibility of lipid detection in vivo by image-guided proton MRS (data not shown).

This study demonstrates the feasibility of an image-guided, voxel-defined technique to quantify CE in human atherosclerotic plaque in ex vivo specimens. In addition to such applications, we are refining this method to localize CE in smaller plaques in an animal model of controlled plaque rupture, as previously described in our study of atherothrombosis in vivo (41). This work has served as a platform on which in vivo studies will be further developed, and if successfully translated to the clinical realm, may serve as a noninvasive means to identify features of vulnerable atherosclerotic plaque.

This work was supported by National Institutes of Health Grants T32 HL-07224-29 (F.L.R.), R01 HL-067188-04 (J.A.H.), and P01 HL-55993, HL-58976, and HL-61759 (J.L.). The authors thank Dr. Kevin Hallock for helpful comments during the preparation of the manuscript.

REFERENCES

1. Naghavi, M., P. Libby, E. Falk, S. W. Casscells, S. Litovsky, J. Rumberger, J. J. Badimon, C. Stefanadis, P. Moreno, G. Pasterkamp, et al. 2003. From vulnerable plaque to vulnerable patient: a call for new definitions and risk assessment strategies: part I. *Circulation.* **108:** 1664–1672.
2. Libby, P., P. Ridker, and A. Maseri. 2002. Inflammation and atherosclerosis. *Circulation.* **105:** 1135–1143.
3. Fayad, Z. A., and V. Fuster. 2001. Clinical imaging of the high-risk or vulnerable atherosclerotic plaque. *Circ. Res.* **89:** 305–316.
4. Choudhury, R. P., V. Fuster, and Z. A. Fayad. 2004. Molecular, cellular and functional imaging of atherothrombosis. *Nat. Rev. Drug Discov.* **3:** 913–925.
5. Yuan, C., and W. S. Kerwin. 2004. MRI of atherosclerosis. *J. Magn. Reson. Imaging.* **19:** 710–719.
6. Fuster, V., and R. J. Kim. 2005. Frontiers in cardiovascular magnetic resonance. *Circulation.* **112:** 135–144.
7. Yuan, C., L. M. Mitsumori, M. S. Ferguson, N. L. Polissar, D. Echelard, G. Ortiz, R. Small, J. W. Davies, W. S. Kerwin, and T. S. Hatsukami. 2001. In vivo accuracy of multispectral magnetic resonance imaging for identifying lipid-rich necrotic cores and intraplaque hemorrhage in advanced human carotid plaques. *Circulation.* **104:** 2051–2056.
8. Cappendijk, V. C., K. B. J. M. Cleutjens, A. G. H. Kessels, S. Heeneman, G. W. H. Schurink, R. J. T. J. Welten, W. H. Mess, M. J. A. P. Daemen, J. M. A. van Engelshoven, and M. E. Kooi. 2005. Assessment of human atherosclerotic carotid plaque components with multisequence MR imaging: initial experience. *Radiology.* **234:** 487–492.
9. Shinnar, M., J. T. Fallon, S. Wehrli, M. Levin, D. Dalmacy, Z. A. Fayad, J. J. Badimon, M. Harrington, E. Harrington, and V. Fuster. 1999. The diagnostic accuracy of ex vivo MRI for human atherosclerotic plaque characterization. *Arterioscler. Thromb. Vasc. Biol.* **19:** 2756–2761.
10. Sirol, M., V. V. Itskovich, V. Mani, J. G. S. Aguinaldo, J. T. Fallon, B. Misselwitz, H.-J. Weinmann, V. Fuster, J-F. Toussaint, and Z. A. Fayad. 2004. Lipid-rich atherosclerotic plaques detected by gadofluorine-enhanced in vivo magnetic resonance imaging. *Circulation.* **109:** 2890–2896.
11. Wasserman, B. A., W. I. Smith, H. H. Trout III, R. O. Cannon III, R. S. Balaban, and A. E. Arai. 2002. Carotid artery atherosclerosis: in vivo morphologic characterization with gadolinium-enhanced double-oblique MR imaging—initial results. *Radiology.* **223:** 566–573.
12. Small, D. M. 1988. George Lyman Duff memorial lecture. Progression and regression of atherosclerotic lesions. Insights from lipid physical biochemistry. *Arteriosclerosis.* **8:** 103–129.
13. Smith, E. B., and R. S. Slater. 1972. Relationship between low-density lipoprotein in aortic intima and serum-lipid levels. *Lancet.* **1:** 463–469.
14. Seo, T., K. Qi, C. Chang, Y. Liu, T. S. Worgall, R. Ramakrishnan, and R. J. Deckelbaum. 2005. Saturated fat-rich diet enhances selective uptake of LDL cholesteryl esters in the arterial wall. *J. Clin. Invest.* **115:** 2214–2222.
15. Smith, E. B. 1974. The relationship between plasma and tissue lipids in human atherosclerosis. *Adv. Lipid Res.* **12:** 1–49.
16. Leitinger, N. 2003. Cholesteryl ester oxidation products in atherosclerosis. *Mol. Aspects Med.* **24:** 239–250.
17. Felton, C. V., D. Crook, M. J. Davies, and M. F. Oliver. 1997. Relation of plaque lipid composition and morphology to the stability of human aortic plaques. *Arterioscler. Thromb. Vasc. Biol.* **17:** 1337–1345.
18. Forder, J. R., and G. M. Pohost. 2003. Cardiovascular nuclear magnetic resonance: basic and clinical applications. *J. Clin. Invest.* **111:** 1630–1639.
19. Soila, K., P. Nummi, T. Ekfors, M. Viamonte, Jr., and M. Kormano. 1986. Proton relaxation times in arterial wall and atheromatous lesions in man. *Invest. Radiol.* **21:** 411–415.
20. Hamilton, J. A., and J. D. Morrisett. 1986. Nuclear magnetic resonance studies of lipoproteins. *In* Methods in Enzymology. J. P. Segrest and J. J. Albers, editors. Academic Press, Orlando, FL. 472–515.
21. Waugh, D. A., and D. M. Small. 1984. Identification and detection of in situ cellular and regional differences of lipid composition and class in lipid-rich tissue using hot stage polarizing light microscopy. *Lab. Invest.* **51:** 702–714.
22. Higgins, C. L., S. A. Marvel, and J. D. Morrisett. 2005. Quantification of calcification in atherosclerotic lesions. *Arterioscler. Thromb. Vasc. Biol.* **25:** 1567–1576.
23. Kawasaki, M., H. Takatsu, T. Noda, K. Sano, Y. Ito, K. Hayakawa, K. Tsuchiya, M. Arai, K. Nishigaki, G. Takemura, et al. 2002. In vivo quantitative tissue characterization of human coronary arterial plaques by use of integrated backscatter intravascular ultrasound and comparison with angioscopic findings. *Circulation.* **105:** 2487–2492.
24. Jang, I-K., G. J. Tearney, B. MacNeill, M. Takano, F. Moselewski, N. Iftima, M. Shishkov, S. Houser, H. T. Aretz, E. F. Halpern, et al. 2005. In vivo characterization of coronary atherosclerotic plaque by use of optical coherence tomography. *Circulation.* **111:** 1551–1555.
25. Kampschulte, A., M. S. Ferguson, W. S. Kerwin, N. L. Polissar, B. Chu, T. Saam, T. S. Hatsukami, and C. Yuan. 2004. Differentiation of intraplaque versus juxtaluminal hemorrhage/thrombus in advanced human carotid atherosclerotic lesions by in vivo magnetic resonance imaging. *Circulation.* **110:** 3239–3244.
26. Petersen, K. F., D. Befroy, S. Dufour, J. Dziura, C. Ariyan, D. L. Rothman, L. DiPietro, G. W. Cline, and G. I. Shulman. 2003. Mitochondrial dysfunction in the elderly: possible role in insulin resistance. *Science.* **300:** 1140–1142.
27. Reingold, J. S., J. M. McGavock, S. Kaka, T. Tillery, R. G. Victor, and L. S. Szczepaniak. 2005. Determination of triglyceride in the human myocardium by magnetic resonance spectroscopy: reproducibility and sensitivity of the method. *Am. J. Physiol. Endocrinol. Metab.* **289:** E935–E939.
28. Perseghin, G., P. Scifo, F. De Cobelli, E. Pagliato, A. Battezzati, C. Arcelloni, A. Vanzulli, G. Testolin, G. Pozza, A. Del Maschio, et al. 1999. Intramyocellular triglyceride content is a determinant of in vivo insulin resistance in humans: a 1H–13C nuclear magnetic resonance spectroscopy assessment in offspring of type 2 diabetic parents. *Diabetes.* **48:** 1600–1606.
29. Szczepaniak, L. S., P. Nurenberg, D. Leonard, J. D. Browning, J. S. Reingold, S. Grundy, H. H. Hobbs, and R. L. Dobbins. 2005. Magnetic resonance spectroscopy to measure hepatic triglyceride content: prevalence of hepatic steatosis in the general population. *Am. J. Physiol. Endocrinol. Metab.* **288:** E462–E468.

30. Katz, S. S., and D. M. Small. 1980. Isolation and and partial characterization of the lipid phases of human atherosclerotic plaques. *J. Biol. Chem.* **255:** 9753–9759.
31. Hamilton, J. A., C. Talkowski, E. Williams, E. M. Avila, A. Allerhand, E. H. Cordes, and G. Camejo. 1973. Natural abundance carbon-13 nuclear magnetic resonance spectra of human serum lipoproteins. *Science.* **180:** 193–195.
32. Hamilton, J. A., E. H. Cordes, and C. J. Glueck. 1979. Lipid dynamics in human low density lipoproteins and human aortic tissue with fibrous plaques. A study by high field 13C NMR spectroscopy. *J. Biol. Chem.* **254:** 5435–5441.
33. Guo, W., J. D. Morrisett, M. E. DeBakey, G. M. Lawrie, and J. A. Hamilton. 2000. Quantification in situ of crystalline cholesterol and calcium phosphate hydroxyapatite in human atherosclerotic plaques by solid-state magic angle spinning NMR. *Arterioscler. Thromb. Vasc. Biol.* **20:** 1630–1636.
34. Guo, W., and J. A. Hamilton. 1996. 13C MAS NMR studies of crystalline cholesterol and lipid mixtures modeling atherosclerotic plaques. *Biophys. J.* **71:** 2857–2868.
35. Zajicek, J., J. D. Pearlman, M. B. Merickel, C. R. Ayers, J. R. Brookeman, and M. F. Brown. 1987. High-resolution proton NMR spectra of human arterial plaque. *Biochem. Biophys. Res. Commun.* **149:** 437–442.
36. Pearlman, J. D., J. Zajicek, M. B. Merickel, C. S. Carman, C. R. Ayers, J. R. Brookeman, and M. F. Brown. 1988. High-resolution 1H NMR spectral signature from human atheroma. *Magn. Reson. Med.* **7:** 262–279.
37. Maynor, C. H., H. C. Charles, R. J. Herfkens, S. A. Suddarth, and G. A. Johnson. 1989. Chemical shift imaging of atherosclerosis at 7.0 Tesla. *Invest. Radiol.* **24:** 52–60.
38. Mohiaddin, R. H., D. N. Firmin, S. R. Underwood, A. K. Abdulla, R. H. Klipstein, R. S. Rees, and D. B. Longmore. 1989. Chemical shift magnetic resonance imaging of human atheroma. *Br. Heart J.* **62:** 81–89.
39. Vinitski, S., P. M. Consigny, M. J. Shapiro, N. Janes, S. N. Smullens, and M. D. Rifkin. 1991. Magnetic resonance chemical shift imaging and spectroscopy of atherosclerotic plaque. *Invest. Radiol.* **26:** 703–714.
40. Wong, W. F., S. R. Northrup, R. C. Herrick, A. P. Glombicki, R. P. Wood, and J. D. Morrisett. 1994. Quantitation of lipid in biological tissue by chemical shift magnetic resonance imaging. *Magn. Reson. Med.* **32:** 440–446.
41. Johnstone, M. T., R. M. Botnar, A. S. Perez, R. Stewart, W. C. Quist, J. A. Hamilton, and W. J. Manning. 2001. In vivo magnetic resonance imaging of experimental thrombosis in a rabbit model. *Arterioscler. Thromb. Vasc. Biol.* **21:** 1556–1560.